

Dissakisite-(Ce) chemical composition: some implications for its origins

Mihoko Hoshino^{1,*}, Mitsuyoshi Kimata¹, Norimasa Nishida² Masahiro Shimizu¹

¹ Earth Evolution Sciences, Graduate School of Life and Environmental Sciences,
University of Tsukuba, 1-1-1 Tennoudai, Tsukuba, Ibaraki 305-8572, Japan

² Chemical Analysis Division, Research Facility Centre for Science and Technology,
University of Tsukuba, 1-1-1 Tennoudai, Tsukuba, Ibaraki 305-8577, Japan

Present address:

Mineral Resource Research Group, Institute for Geo-Resources and Environment,
National Institute of Advanced Industrial Science and Technology, 1-1-1 Higashi,
Tsukuba, Ibaraki, 305-8567, Japan

*E-mail address: hoshino-m@aist.go.jp

Telephone number : +81-29-861-2474

Fax number : +81-29-861-3717

Abstract

Euhedral dissakisites from Trimouns dolomite mine, France, is compositionally-zoned. Back-scattered electron (BSE) images reveal that each of the described dissakisite crystals has three distinct compositional zones: normal zoned core (Mg-rich), oscillatory zoned middle (Ca-Al-rich) and homogeneous rim (Fe-ΣREE-rich). The latter zone with $Fe^{2+} > Mg$ corresponds to allanite-(Ce). Dissakisite-(Ce) also

displays pronounced zoning in Fe/Mg which may suggest that the temperature of crystallization continuously decreased from core to rim. Despite a systematic increase in Fe/Mg of the dissakisite with an allanite rim, there is no monotonic decrease in the REE zoning: the normal zoned core and homogeneous rim are rich in La, Ce and Pr, but the relatively REE-poor oscillatory zoned middle is relatively abundant in Y, Sm and Gd. Discontinuous variation in REE content of the dissakisite, with the allanite rim may indicate a localized change in either the relative concentration of various ligands or pH of the crystallizing fluid. Observations under the polarizing microscope confirm that the different zones have simultaneous extinction. These chemical and optical observations suggest that epitaxial crystallization of dissakisite, from Trimouns, passes through three formation stages.

The ternary $\text{Fe}^{2+}\text{-Mg}^{2+}\text{-(Al + Fe)}^{3+}$ diagram illustrates that in general dissakisite can be classified into two groups, $(\text{Al + Fe})^{3+}$ -rich and an Mg-rich; Dissakisite from Trimouns belongs to the former group. Chondrite-normalized REE patterns of dissakisites from Trimouns are similar to those of allanites formed by hydrothermal fluids. In conclusion, it is clear from the above two geochemical characteristics that dissakisites from Trimouns are of $(\text{Al + Fe})^{3+}$ -type, and were derived from hydrothermal fluids.

Keywords dissakisite · allanite · rare earth elements · compositional zoning · chondrite-normalized REE pattern · origin

Introduction

Dissakisite-(Ce) is a Mg analogue of allanite, with the ideal formula $\text{CaCeMgAl}_2\text{Si}_3\text{O}_{12}(\text{OH})$, which has been reported from some metamorphic occurrences (Grew et al. 1991; Enami and Zang 1988; Zakrzewski et al. 1992; De Parseval et al. 1997; Marty 2004). To date, the only occurrence of Cr-rich dissakisite-(Ce) has been reported in a garnet lherzolite (Yang and Enami 2003), and the discovery of (Th, Cr)-bearing cerian dissakisite-(La) occurring in a peridotite body has led to the acceptance of a new mineral species dissakisite-(La) by the IMA Commission (Tumiati et al. 2005). Compositional zoning of dissakisite-(Ce) from Trimouns and Balchen Mountain (type locality) was first observed by Hoshino et al. (2008), but compositional zones have been known to present in both Cr-rich dissakisite-(Ce) (Yang and Enami 2003) and dissakisite-(La) (Tumiati et al. 2005). However, the constraints on the chemical variation of dissakisite are poorly understood, and relatively few systematic investigations of its chemical composition have been made.

In this paper, we report the description of compositionally-zoned dissakisite. Both the constraints on chemical composition of dissakisite and their implications for genesis of dissakisite are discussed in terms of rare earth element (REE) patterns.

Experimental methods

Sample description

The sample described in this study was dissakisite in a dolomite lens from the talc-chlorite deposit of Trimouns in the French Pyrenees (De Parseval et al. 1997; Marty 2004; Hoshino et al. 2008). Dissakisites appear to be well-crystallized and occur as brown euhedral crystals (ranging in size from $0.5 \times 0.8 \times 3.0$ mm to $1.0 \times 1.5 \times 5.0$

mm).

Electron Microprobe Analyses (EMPA)

Chemical analyses were performed using the JEOL JAX-8621 electron microprobe equipped with three wavelength-dispersion spectrometers (WDS) at the Chemical Analysis Division, University of Tsukuba. Compositional zones were observed in back-scattered electron (BSE) images, an example of which is shown in Fig. 1. Details of the analyses have been provided by Hoshino et al. (2005, 2008). Representative analyses of the zones are presented in Table 1. Chemical formulae were calculated on the basis of 12 O + OH and all Fe was assumed to be Fe²⁺ (Grew et al. 1991; De Parseval et al. 1997; Hoshino et al. 2008).

Results

Chemical composition

The dissakisite is compositionally-zoned and observed in BSE images (Fig. 1). The crystal displays a series of compositionally distinct zones that reflect an overgrowth of different types of dissakisite. Moreover, the zoning is characterised by straight boundary limits, and divided into three zones; normal zoned core, oscillatory zoned middle and homogeneous rim (Fig. 1). The normal zoned core (Fig. 1) is visually similar to the magmatic zoning evidenced by marking several different levels of composition with straight boundary limits (Gieré and Sorensen 2004). The oscillatory zone in this study has fine growth bands. The thickness of the oscillations remarkably

increases from core to rim. Furthermore, close observation of these zones under the polarizing microscope reveals that they have simultaneous extinction with one another (Fig. 1).

EMPA traverses and quantitative analyses reveal the presence of a Mg-rich core, Ca-Al-rich middle and Fe-ΣREE-rich rim (Table 1 and Fig. 2). Quantitative EMPA of each zone demonstrate that Ce predominates over both La and all other REE and that these minerals from Trimouns correspond to dissakisite-(Ce) (Table 1). However, the homogeneous rim zones, with $Fe^{2+} > Mg$ are identified as allanite-(Ce) (Table 1; 8-10) from the classification of epidote group minerals employed by Grew et al. (1991). Our study here is the first report of both the rim of allanite-(Ce) and the middle zone of oscillatory zoning observed for the present dissakisite-(Ce). Although the zoning of the present dissakisite is complex (Fig. 1), REE contents in the rim zone or allanite-(Ce), are the highest of the three zones (Table 1). Moreover, EMPA traverse and quantitative analyses reveal that there is no monotonic decrease in the REE zoning of the present dissakisite with allanite rim: the normal zoned core and homogeneous rim are rich in La, Ce and Pr, but the relatively REE-poor oscillatory zoned middle is relatively abundant in Y, Sm and Gd (Table 1, Figs. 1 and 2).

Discussion

Compositional zoning in dissakisite-(Ce)

Allanite is known to exhibit three types of chemical zoning, as revealed in BSE images: (1) oscillatory zoning (e.g., Buda and Nagy 1995), (2) normal growth-induced magmatic zoning (e.g., Gieré and Sorensen 2004), and (3) patchy zoning (e.g., Petřík et

al. 1995). Type (1) was interpreted as providing evidence for the crystal growth of this mineral from the melt (e.g., Gromet and Silver 1983). Allanites often occur with types (2) and/or (3) in many metamorphic and hydrothermal environments (e.g., Sorensen 1991; Catlos et al. 2000; Poitrasson 2002). Here, the zoning is primarily due either to release or consumption of REE during the metamorphic reactions involving other REE minerals or to multiple interactions with hydrothermal fluids of variable REE contents (e.g., Exley 1980; Smith et al. 2002). Some previous studies of dissakisite reported minor zoning (Yang and Enami 2003), strongly zoned rims (Tumiati et al. 2005) and normal growth-induced magmatic zoning (Hoshino et al. 2008). The former two appear to be formed by metamictization. BSE images of dissakisite in our study reveal the existence of normal zoned core, oscillatory middle and homogeneous rim (Fig. 1). Therefore, the present combination of normal zoned core, oscillatory middle and homogeneous rim appear to be unique among epidote group minerals, commonly observed in those from Trimouns (Fig. 1a in Hoshino et al. 2008). Although total REE contents in our present study decreases from core to middle, the total REE content is the highest of the three zones (Table 1). Therefore, the present compositional zoning in the core to middle of dissakisite with allanite rim is of the normal type that REE contents decrease from the core to the rim. On the other hand the increase of REE contents from dissakisite middle to allanite rim represents a reverse type (Figs.1 and 2). For example, the reverse zoning of allanite from the Catalina migmatites seems to indicate that REE were added to the rock volumes during the mineral growth (Sorensen 1991). A decrease in Fe/Mg from core to rim of a garnet grain has been interpreted as due to crystallization with increasing temperature (Ghent et al. 1987). In our study, dissakisite-(Ce) also displays a pronounced zoning in both Fe/Mg ratio and Fe versus

Mg diagram (Table 1 and Fig. 3), which may suggest that the temperature of crystallization decreased continuously from core to rim. Despite a systematic increase in Fe/Mg ratio, there is no monotonic decrease in the REE zoning: the normal zoned core and homogeneous rim are rich in La, Ce and Pr, but the relatively REE-poor oscillatory zoned middle is fairly abundant in Y, Sm and Gd (Table 1, Figs. 2 and 4). The concentrations of these relatively middle- to heavy-REE initially increase as the total REE decreases (Table 1, Figs. 2 and 4). A variety of ligands, including F⁻, Cl⁻, OH⁻, SO₄²⁻ and CO₃²⁻, are likely candidates for complexing the REE in hydrothermal fluids (e.g., Hass et al. 1995; Gieré 1996). The speciation of REE in the fluid, however, is not only affected by temperature and pressure but also strongly controlled by both the relative concentration of various ligands and pH of the solution (e.g., Gieré 1996). Moreover, the heavy REE (HREE: Gd-Lu) are complexed more strongly by fluoride, and less strongly by chloride, than the light-REE (LREE: La-Sm), in hydrothermal fluids (e.g., Hass et al. 1995). Therefore, discontinuous variation in REE contents of dissakisite with the allanite rim described here, may suggest a local change in either the relative concentration of various ligands or pH of the solution. Furthermore, Nd, Sm and Y contents increase towards the rims of zoned allanite crystals, which is consistent with the feature reported from several suites of igneous allanites (Sawka et al. 1984; Chesner and Ettlinger 1989; Catlos et al. 2000; Buda and Nagy 1995; Beard et al. 2006). The most reasonable explanation for the marked increase of Nd, Sm and Y in a zoned allanite is that the allanite/melt partition coefficients (K_d values) for REEs can change during the crystallization (Beard et al. 2006). Compared with the change of REE contents in zoned allanites observed by Beard et al. (2006) (REE₂O₃: 1.00-18.67 wt%), that in the present dissakisite with allanite rim (REE₂O₃: 22.49-26.43 wt%) is small

(Table 1). Therefore, as revealed under a polarising microscope, the compositional zones display simultaneous extinction with one another. These optical and chemical observations suggest that crystallization of the dissakisite with allanite rim occurred in three stages, as is also evident from the plots of Fe versus Mg and (La+Ce+Pr) versus (Sm+Gd+Y) for each zone (Figs. 3 and 4), and that the relationship of dissakisite (core-middle zones) to allanite (rim zone), grown steadily with their crystallographic axes mutually parallel to each other, may be identified as epitaxy.

Dissakisite-(Ce) with characteristic chemical compositions

In order to provide some necessary background for crystallization of dissakisites, this study compares both the ternary Fe^{2+} - Mg^{2+} - $(\text{Al} + \text{Fe})^{3+}$ compositions and chondrite-normalized REE patterns of dissakisite with those based on previously published data (Grew et al. 1991; Rouse and Peacor 1993; De Parseval et al. 1997; Yang and Enami 2003; Tumiati et al. 2005; Hoshino et al. 2008). This comparison, as is evident from Figure 5, suggests that dissakisites should be grouped into two classes: an $(\text{Al} + \text{Fe})^{3+}$ -type and a Mg-one. Dissakisite from Trimouns belongs to the former, while those from Balchen Mountain are categorized as the latter. The data for three different zones of dissakisite grain from Trimouns are plotted relatively close to one another, although the homogeneous rim is closer to allanite-(Ce) endmember (Fig. 5). Furthermore, dissakisite from Ulten zone is the $(\text{Al} + \text{Fe})^{3+}$ -type and those from Su-Lu UHP metamorphic terrane the Mg-type, although both occur in peridotites (Fig. 5). The distinction between the two types may reflect a material difference in chemical composition among the host rocks, namely dolomite, marble and peridotite.

REE abundances in dissakisites from several different occurrences can be characterized in terms of chondrite-normalized REE patterns (Fig. 6). To quantify the shape and slope of the REE patterns, the chondrite-normalized ratio of $(La/Sm)_{cn}$ is used using chondrite-normalizing values from McDonough and Sun (1995) (Table 1, Fig. 6). Generally, $(La/Sm)_{cn}$, $(La/Nd)_{cn}$ and $(La/Yb)_{cn}$ ratios in apatite are effective for both the classification of S-type and I-type granites (Sha and Chappell 1999) and the degree of fractionation of carbonatite (Bühn et al. 2001). Therefore, the $(La/Sm)_{cn}$ ratio in dissakisites may reflect better the differences in chemical composition among their host rocks. As demonstrated by chondrite-normalized REE patterns (e.g., Grew et al. 1991; Yang and Enami 2003; Gieré and Sorensen 2004), dissakisite strongly fractionates the LREE from HREE. It is clear from Figs. 6a-c that the flat REE patterns of dissakisite in dolomite from Trimouns are distinct from the relatively fractionated ones of dissakisites in both marble from Balchen Mountain and peridotites from the Chinese Su-Lu-UHP metamorphic terrane and Ulten zone; the $(La/Sm)_{cn}$ values in dissakisites from Trimouns are lower than those from the other occurrences. Gieré (1996) classified the occurrences of hydrothermal allanite into five groups: (1) Alpine-type fissures (e.g., Braun 1997), (2) cavities (e.g., Bromely 1964; no REE data), (3) veins (e.g., Exley 1980; Pan et al. 1994), (4) skarns (e.g., Zakrzewski et al. 1992) and (5) replacement bodies (e.g., Lira and Ripley 1990; no REE data). According to this classification, the present example of dissakisite-(Ce) from Trimouns belongs to the occurrence of Alpine-type fissures. Hydrothermal allanites from both Alpine-type fissures (De Parseval et al. 1997), and vein or microvein of sulfides and silicates transecting the chloritite matrix (Pan et al. 1994), exhibit characteristic REE patterns and $(La/Sm)_{cn}$ ratios which are roughly parallel to those of dissakisite in dolomite from Trimouns (Fig.

6a). In contrast, hydrothermal allanites in both skarn (e.g., Zakrzewski et al. 1992) and calcite vein assemblages (Peterson and MacFarlane 1993), strongly fractionate the LREE from HREE (Fig. 6d). These characteristics suggest that the chondrite-normalized REE patterns of hydrothermal allanite can also be divided into two types (i.e. “Alpine-type fissures and veins and microveins of sulfides and silicates transecting the chloritite matrix type”, “skarn and calcite vein type”), although no occurrences of dissakisites from (2) cavities, (3) veins (4) skarns or (5) replacement bodies have been reported. Therefore, ternary Fe^{2+} - Mg^{2+} - $(\text{Al} + \text{Fe})^{3+}$ compositions and chondrite-normalized REE patterns of dissakisite can provide valuable petrogenetic information for its host rock.

Acknowledgments

The authors would like to thank Prof. E.S. Grew (University of Maine) for his suggestions about this study. The paper benefited greatly from official reviews done by B. Lavina and an anonymous reviewer. This work was funded in 2008 by the Hayashi Memorial Foundation for Female Natural Scientists.

References

- Beard JS, Sorensen SS, Gieré R (2006) REE zoning in allanite related to changing partition coefficients during crystallization: implications for REE behaviour in an epidote-bearing tonalite. *Mineral Mag* 70: 419-435
- Braun MC (1997) REE-Ungleichgewichte in Gesteinen der Lebendun Serie am Monte Giove. Doctoral thesis, Universität Basel, Switzerland
- Bromley AV (1964) Allanite in the Tan-Y-Grisiau Microgranite, Merionethshire, North

- Wales. *Am Mineral* 49: 1747-1752
- Buda G, Nagy G. (1995) Some REE-bearing accessory minerals in two types of Variscan granitoids, Hungary. *Geologica Carpathica* 46: 67-78
- Bühn B, Wall F, Le Bas MJ (2001) Rare-earth element systematics of carbonatitic fluorapatites, and their significance for carbonatite magma evolution. *Contrib Mineral Petrol* 141: 572-591
- Catlos EJ, Sorensen SS, Harrison TM (2000) Th-Pb ion-microprobe dating of allanite. *Am Mineral* 85: 633-648
- Chesner CA, Ettliger AD (1989) Composition of volcanic allanite from the Toba Tuffs, Sumatra, Indonesia. *Am Mineral* 74: 750-758
- De Parseval P, Fontan F, Aigouy T (1997) Chemical composition of REE minerals from Trimouns (French Pyrenees). *Comptes Rendus de l'Académie des Sciences*, Série II : Sciences de la Terre et des Planètes 324 : 625-630
- Enami M, Zang Q (1988) Magnesian staurolite in garnet-corundum rocks and eclogite from the Donghai district, Jiangsu province, east China. *Am Mineral* 73: 48-56
- Exley RA (1980) Microprobe studies of REE-rich accessory minerals: implications for Skye granite petrogenesis and REE mobility in hydrothermal systems. *Earth Planet Sci Lett* 48: 97-110
- Ghent ED, Black PM, Brothers RN, Stout MZ (1987) Eclogites and associated albite-epidote-garnet paragneisses between Yambe and Cape Colnett, New Caledonia. *J Petrol* 28: 627-643
- Gieré R (1996) Formation of rare earth minerals in hydrothermal systems. In: Jones AP, Wall F, Williams CT (eds) *Rare Earth Minerals. Series 7*: 105-150.

The Mineralogical Society, Chapman & Hall, London, U.K.

- Gieré R, Sorensen SS (2004) Allanite and other REE-rich epidote-group minerals. In: Liebscher A, Franz G, (eds) *Epidotes. Reviews in Mineralogy and Geochemistry* 56: 431-493., Mineralogical Society of America and Geochemical Society, Chantilly, Virginia.
- Grew ES, Essene EJ, Peacor DR, SU S-C, Asami M (1991) Dissakisite-(Ce), a new member of the epidote group and the Mg analogue of allanite-(Ce), from Antarctica. *Am Mineral* 76: 1990-1997
- Gromet LP, Silver LT (1983) Rare earth element distributions among minerals in a granodiorite and their petrogenetic implications. *Geochim Cosmochim Acta*, 47: 925-939
- Hass JR, Shock EL, Sassani DC (1995) Rare earth elements in hydrothermal systems: Estimates of standard partial molal thermodynamic properties of aqueous complexes of the rare earth elements at high pressures and temperatures. *Geochim Cosmochim Acta* 59: 4329-4350
- Hoshino M, Kimata M, Nishida N, Kyono A, Shimizu M, Takizawa S (2005) The chemistry of allanite from the Daibosatsu Pass, Yamanashi, Japan. *Mineral Mag* 69: 403-423
- Hoshino M, Kimata M, Nishida N, Shimizu M (2008) Crystal chemical significance of chemical zoning in dissakisite-(Ce). *Phys Chem Minerals* 35: 59-70
- Lira R, Ripley EM (1990) Fluid inclusion studies of the Rodeo de Los Molles REE and Th deposit, Las Chacras Batholith, Central Argentina. *Geochim Cosmochim Acta* 54: 663-671
- Marty F (2004) The Trimouns Quarry Luzenac, Ariège, France. *Mineral Record* 35:

225-247

McDonough WF, Sun S-s (1995) The composition of the Earth. *Chem Geol* 120:

223-253

Pan Y, Fleet ME, Barnett RL (1994) Rare-earth mineralogy and geochemistry of the

Mattagami lake volcanogenic massive sulfide deposit, Quebec. *Can Mineral* 32:

133-147

Peterson RC, MacFarlane DB (1993) The rare-earth-element chemistry of allanite from

the Grenville Province. *Can Mineral* 31: 159-166

Petrík I, Broska I, Lipka J, Šiman P (1995) Granitoid allanite-(Ce): substitution

relations, redox conditions and REE distributions (on an example of I-type

granitoids, western Carpathians, Slovakia). *Geologica Carpathica* 46: 79-94

Poitrasson F (2002) In situ investigations of allanite hydrothermal alteration:

examples from calc-alkaline and anorogenic granites of Corsica (southeast France).

Contrib Mineral Petrol 142: 485-500

Rouse RC, Peacor DR (1993) The crystal structure of dissakisite-(Ce), the Mg

analogue of allanite-(Ce). *Can Mineral* 31: 153-157

Sawka WN, Chappell BW, Norrish K, (1984) Light-rare-element zoning in sphene and

allanite during granitoid fractionation. *Geology* 12: 131-134

Sha L-K, Chappell BW, (1999) Apatite chemical composition, determined by electron

microprobe and laser-ablation inductively coupled plasma mass spectrometry, as a

probe into granite petrogenesis. *Geochim Cosmochim Acta* 63: 3861-3881

Sorensen SS (1991) Petrogenetic significance of zoned allanite in garnet amphibolites

from a paleo-subduction zone: Catalina Schist, southern California. *Am*

Mineral 76: 589-601

- Smith MP, Henderson P, Jeffries T (2002) The formation and alteration of allanite in skarn from the Beinn an Dubhaich granite aureole, Skye. *Eur J Mineral* 14: 471-486
- Tumiati S, Godard G, Martin S, Nimis P, Mair V, Boyer B (2005) Dissakisite-(La) from the Ulten zone peridotite (Italian Eastern Alps): A new end-member of the epidote group. *Am Mineral* 90: 1177-1185
- Yang J-J, Enami M (2003) Chromian dissakisite-(Ce) in a garnet lherzolite from the Chinese Su-Lu UHP metamorphic terrane: implications for Cr incorporation in epidote-group minerals and recycling of REE into the Earth's mantle. *Am Mineral* 88: 604-610
- Zakrzewski MA, Lustenhouwer WJ, Nugteren HJ, Williams CT (1992) Rare-earth minerals yttrian zirconolite and allanite-(Ce)* and associated minerals from Koberg mine, Bergslagen, Sweden. *Mineral Mag* 56: 27-35

Table 1. Electron microprobe analyses of dissakisites from Trimouns (1-4: normal zoned core, 5-7: oscillatory zoned middle, 8-10: homogeneous rim)

spot ^a n ^b	Normal zoned core				Oscillatory zoned middle			Homogeneous rim		
	1	2	3	4	5	6	7	8	9	10
SiO ₂	32.1(3)	32.7(9)	32.5(4)	32.8(3)	33.2(2)	33.2(2)	33.4(1)	30.7(4)	31.9(6)	31.5(1)
TiO ₂	0.38(2)	0.27(3)	0.25(5)	0.22(2)	0.20(2)	0.16(4)	0.16(3)	0.17(1)	0.16(2)	0.20(4)
Al ₂ O ₃	19.0(2)	19.26(7)	19.83(6)	19.68(0)	20.40(7)	21.0(5)	21.14(9)	18.75(1)	18.4(9)	18.7(2)
Y ₂ O ₃	0.13(1)	0.15(2)	0.11(1)	0.17(3)	0.18(1)	0.26(3)	0.34(1)	<0.04	0.05(2)	<0.04
La ₂ O ₃	6.65(6)	5.8(1)	5.87(5)	5.50(1)	4.4(7)	4.16(7)	4.13(4)	5.6(2)	5.5(9)	5.9(1)
Ce ₂ O ₃	10.4(1)	10.07(6)	9.08(4)	9.76(7)	8.85(3)	8.0(2)	7.9(1)	10.92(8)	10.4(8)	11.18(1)
Pr ₂ O ₃	1.67(7)	1.70(7)	1.66(6)	1.7(1)	1.57(3)	1.56(1)	1.61(2)	1.85(5)	1.82(4)	1.87(5)
Nd ₂ O ₃	5.5(5)	6.37(6)	5.96(1)	6.45(2)	6.3(4)	6.2(2)	6.13(5)	6.2(1)	6.3(5)	6.2(8)
Sm ₂ O ₃	1.0(1)	1.19(6)	1.17(0)	1.36(2)	1.4(1)	1.45(4)	1.53(0)	1.02(3)	1.07(2)	0.95(8)
Gd ₂ O ₃	0.4(1)	0.48(3)	0.61(4)	0.73(1)	0.7(1)	0.90(1)	0.98(3)	0.35(6)	0.4(2)	0.3(8)
FeO ^c	3.9(2)	3.80(7)	3.17(1)	3.9(2)	3.59(6)	3.77(4)	3.49(3)	8.0(5)	7.5(3)	8.4(3)
MnO	<0.028	<0.028	<0.028	<0.028	<0.028	<0.028	<0.028	0.03(1)	0.04(1)	<0.028
MgO	5.7(4)	5.77(2)	5.3(8)	5.5(6)	5.0(5)	4.6(1)	4.52(7)	2.7(2)	3.12(2)	2.6(4)
CaO	10.81(8)	10.7(1)	11.48(9)	11.19(3)	12.2(2)	12.8(2)	12.84(6)	10.7(1)	10.8(8)	10.6(3)
H ₂ O (calc) ^d	1.64	1.65	1.64	1.66	1.67	1.69	1.69	1.59	1.60	1.60
Total	99.28	99.91	98.63	100.62	99.66	99.75	99.86	98.58	99.06	100.00
Normalized on the basis of 12O + (OH)										
Si	2.958(5)	2.978(2)	2.97(9)	2.97(6)	2.99(7)	2.967(2)	2.977(0)	2.93(4)	2.993(4)	2.96(6)
Ti	0.027(5)	0.019(1)	0.017(3)	0.015(2)	0.013(2)	0.011(3)	0.011(0)	0.012(1)	0.011(1)	0.014(3)
Al	2.06(1)	2.07(1)	2.14(2)	2.098(3)	2.164(7)	2.219(7)	2.223(6)	2.11(2)	2.04(9)	2.07(1)
Y	0.007(0)	0.007(0)	0.005(1)	0.004(1)	0.004(1)	0.013(2)	0.016(1)	0.000	0.003(1)	0.000
La	0.226(8)	0.196(9)	0.198(3)	0.183(0)	0.15(4)	0.137(7)	0.136(2)	0.20(2)	0.19(9)	0.205(5)
Ce	0.349(2)	0.336(5)	0.304(4)	0.323(5)	0.292(2)	0.26(2)	0.259(7)	0.38(1)	0.36(6)	0.385(4)
Pr	0.056(6)	0.056(5)	0.055(4)	0.056(8)	0.051(3)	0.051(1)	0.052(1)	0.064(2)	0.062(0)	0.064(3)
Nd	0.18(3)	0.208(4)	0.195(1)	0.208(1)	0.20(3)	0.20(1)	0.195(2)	0.211(7)	0.21(3)	0.21(8)
Sm	0.03(1)	0.037(4)	0.037(0)	0.042(1)	0.04(1)	0.045(3)	0.047(0)	0.034(2)	0.03(1)	0.031(6)
Gd	0.012(7)	0.015(2)	0.019(2)	0.022(0)	0.02(1)	0.027(1)	0.029(2)	0.011(3)	0.01(1)	0.01(5)
Fe ²⁺	0.298(8)	0.290(8)	0.243(8)	0.291(8)	0.270(7)	0.282(7)	0.260(1)	0.640(8)	0.588(7)	0.658(5)
Mn	0.000	0.000	0.000	0.000	0.000	0.000	0.000	0.003(0)	0.003(0)	0.000
Mg	0.78(9)	0.784(6)	0.72(9)	0.74(9)	0.67(9)	0.61(5)	0.60(2)	0.39(6)	0.44(8)	0.36(9)
Ca	1.07(3)	1.04(2)	1.13(1)	1.085(3)	1.17(3)	1.22(2)	1.223(4)	1.087(8)	1.09(9)	1.07(5)
Sum REE	0.86	0.86	0.81	0.84	0.76	0.73	0.73	0.90	0.87	0.91
Sum Cat	8.05	8.04	8.03	8.04	8.03	8.04	8.03	8.07	8.03	8.04
OH (stoich)	1.00	1.00	1.00	1.00	1.00	1.00	1.00	1.00	1.00	1.00
Fe/Mg	0.38	0.37	0.34	0.39	0.40	0.46	0.43	1.64	1.34	1.83
(La/Sm) _{cn} ^e	4.32	3.03	3.10	2.50	1.97	1.77	1.67	3.40	3.19	3.84

^a See Fig. 1 for spot locations^b Number of microprobe points; number in parenthesis is standard deviation^c All Fe as assumed to Fe²⁺^d Calculated assuming 12 O + (OH)^e (La/Sm)_{cn}: chondrite-normalized ratio of La and Sm (e.g., Sha and Chappell 1999; Bühn et al. 2001)

Figure 1

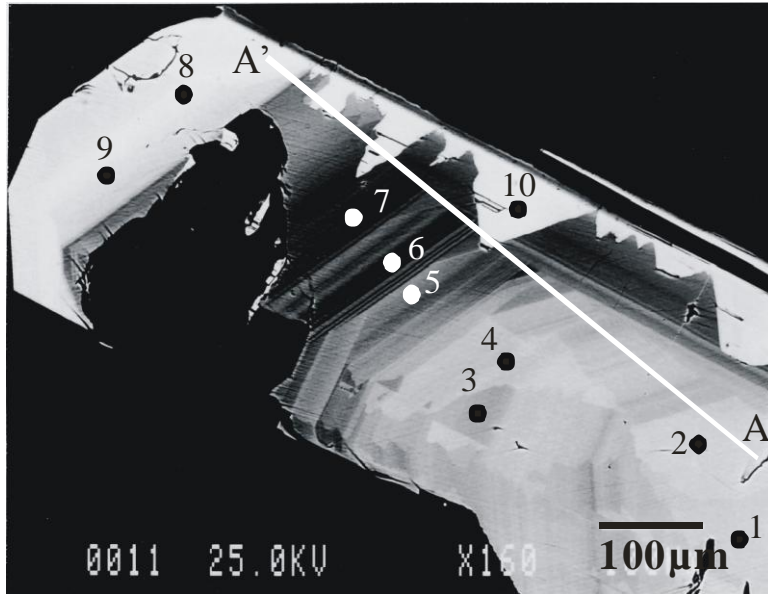


Fig. 1 Back-scattered electron image of dissakisite: chemical-zoned dissakisite from Trimouns. The white line (from A to A') is indicative of the traverse analytical path in Fig.2. The numbered solid circles denote the locations of electron-microprobe analyses, corresponding to the numbers in Table 1.

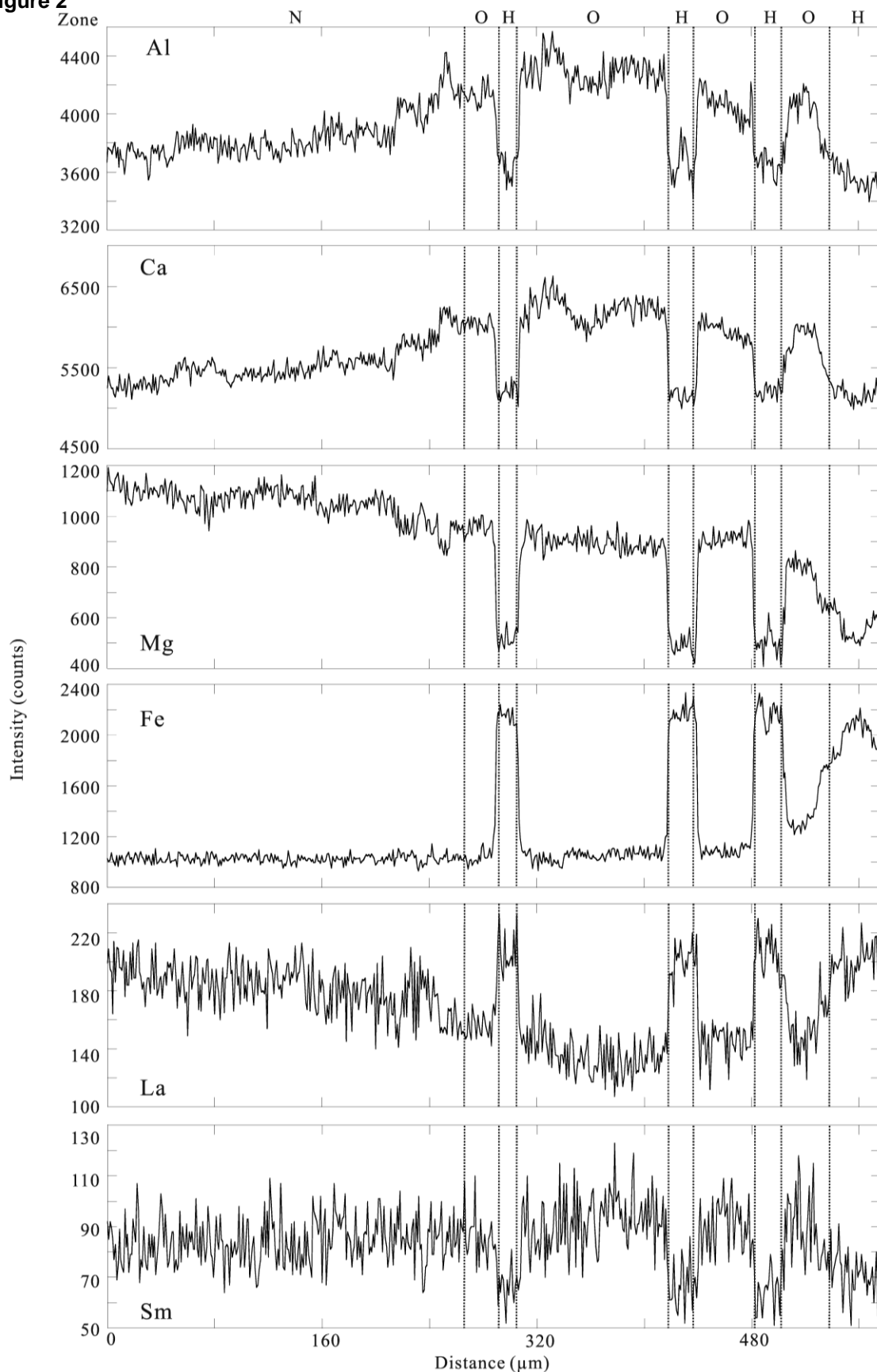
Figure 2

Fig. 2 Variation in Al, Ca, Mg, Fe, La and Sm contents across chemical-zoned dissakisite from Trimouns. The traverse path is 576 μm as shown in Fig. 1 (from start point A to end point A'). Although variations in Ce, Pr and Gd contents are not shown in this figure, those in the first two correspond to that in La, while the third has the same variation as Sm. Each dwelling that is marked by vertical dotted lines is divided into areas of three zone types (N: normal zoned core, O: oscillatory zoned middle and H: homogeneous rim).

Figure 3

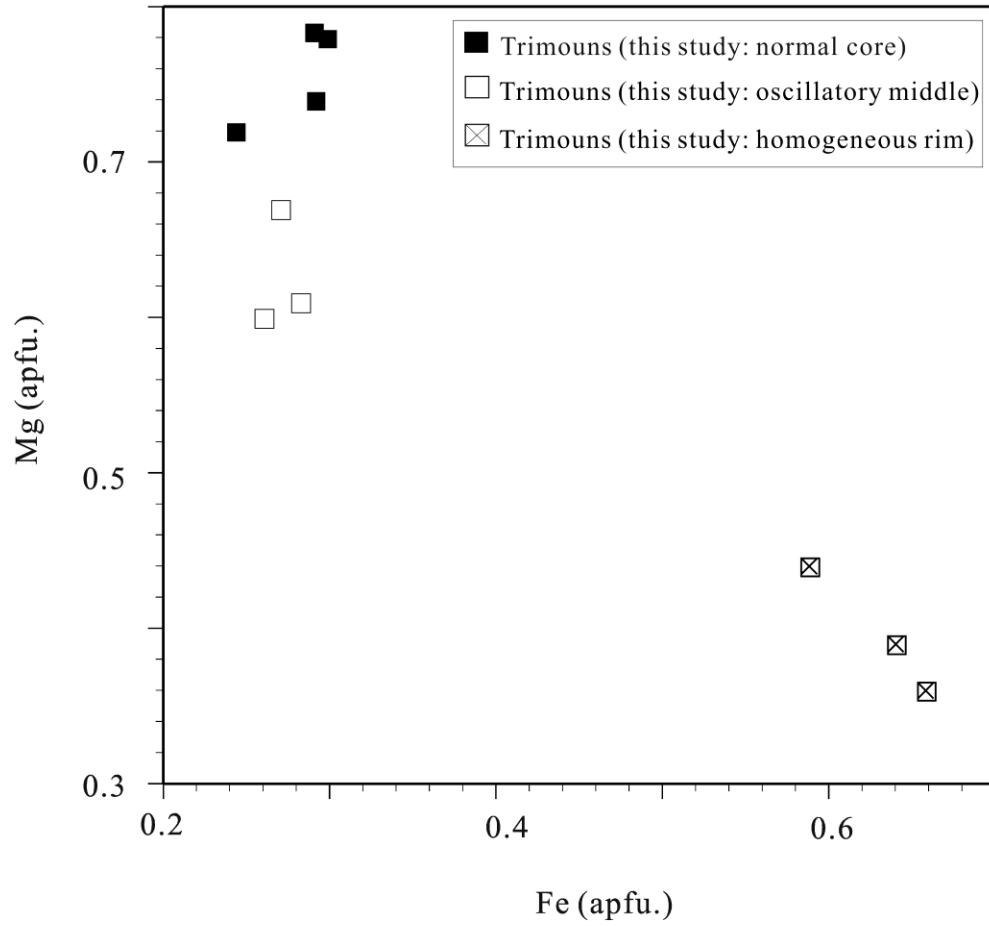


Fig. 3 Plot of Fe versus Mg for the present zoned dissakisite, suggesting systematic change from core to rim. Units are atoms per formula unit (apfu.).

Figure 4

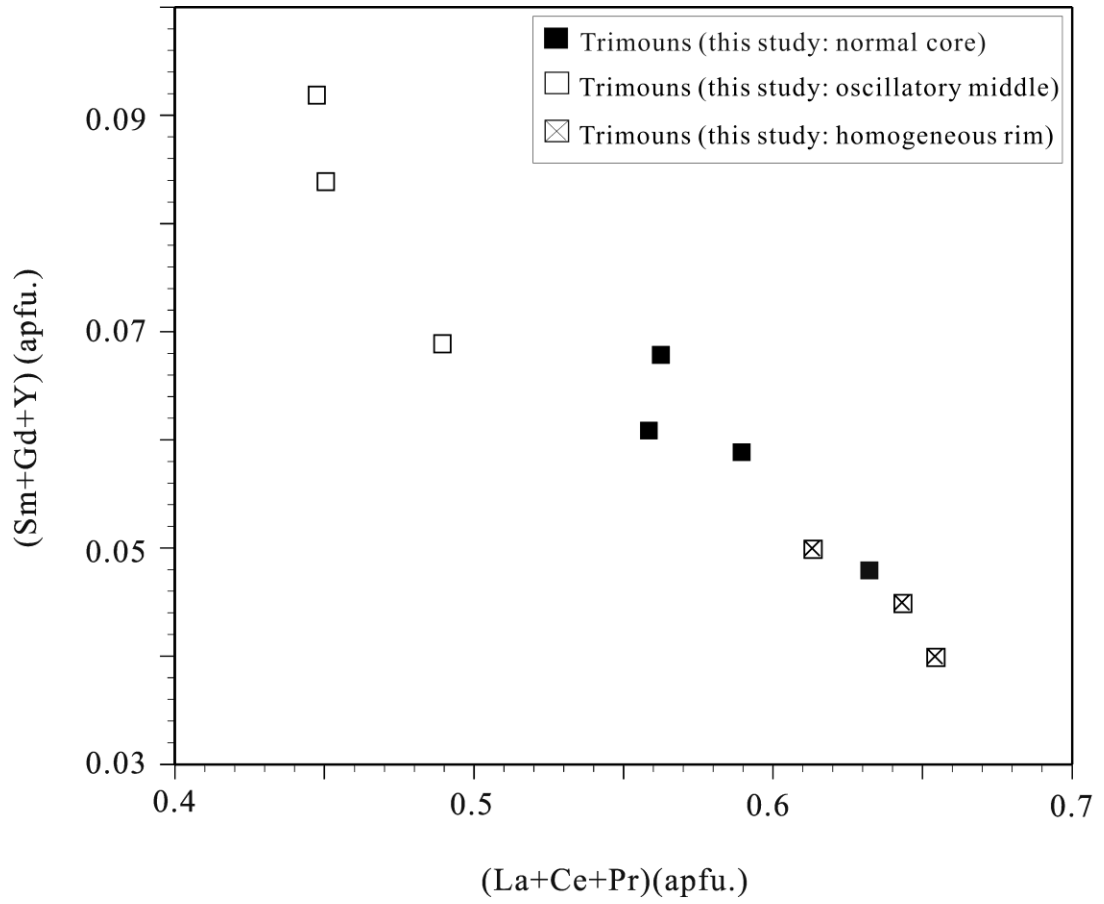
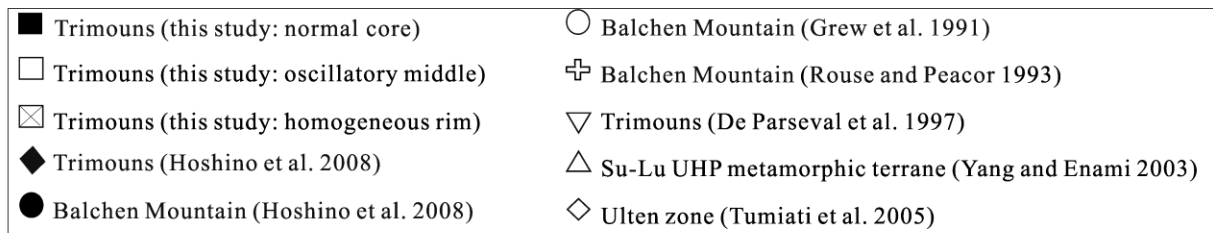


Fig. 4 Plot of (La+Ce+Pr) versus (Y+Sm+Gd) for the present zoned dissakisite, suggesting discontinuously change from core to rim. Units are atoms per formula unit (apfu.).

Figure 5



Epidote, Clinozoisite, Oxyallanite

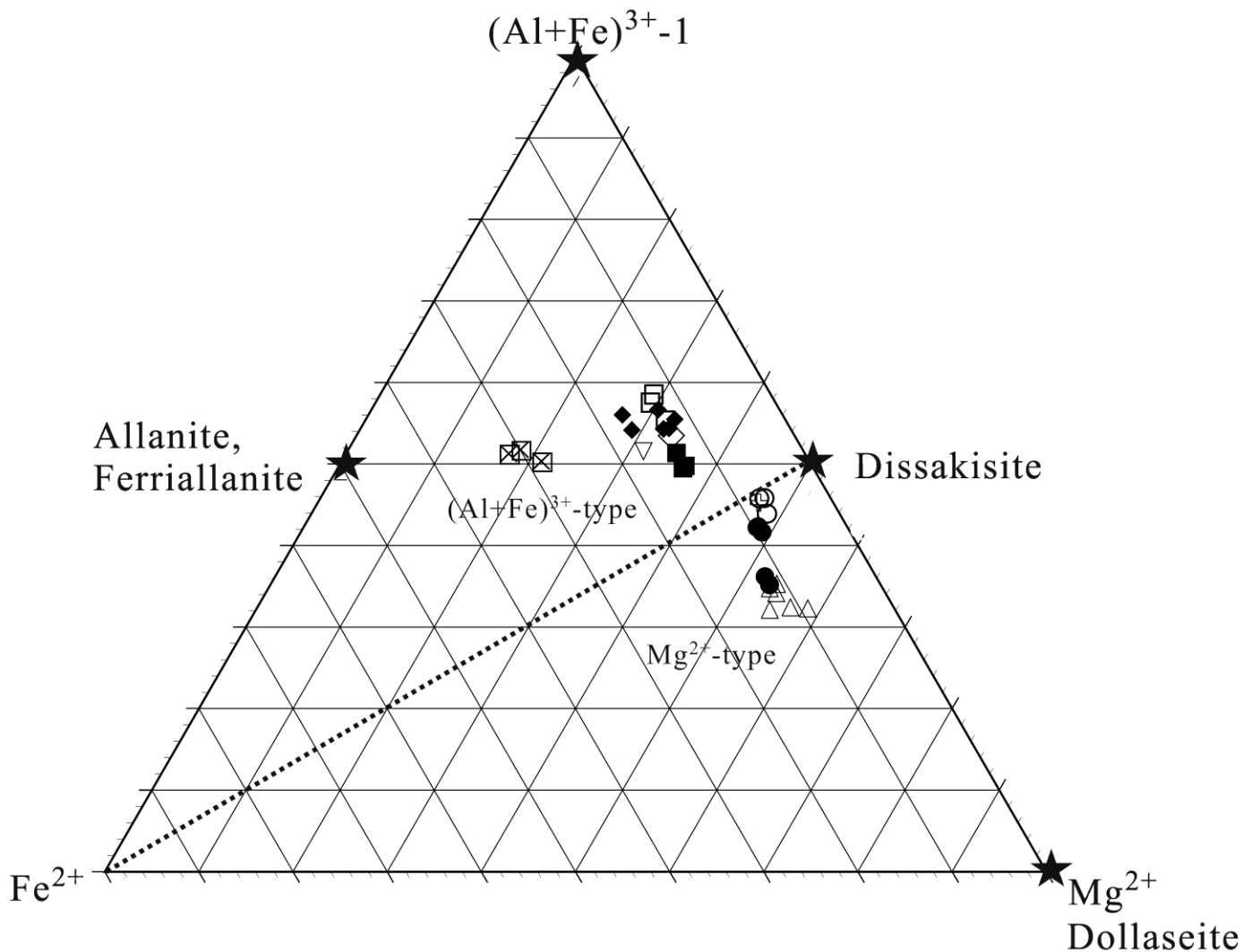


Fig. 5 The extent of solid solutions in Fe^{2+} - Mg^{2+} - $(Al+Fe)^{3+}$ subsystem. This ternary diagram, introduced by Gieré and Sorensen (2004), can be used to show the relationship among epidote-clinozoisite-oxyallanite, allanite-ferriallanite, dollaseite and dissakisite. Asterisks indicate projections of endmember compositions on the diagram. The dashed line shows the boundary between $(Al+Fe)^{3+}$ - and Mg -type dissakisites. Units are atoms per formula unit (apfu.).

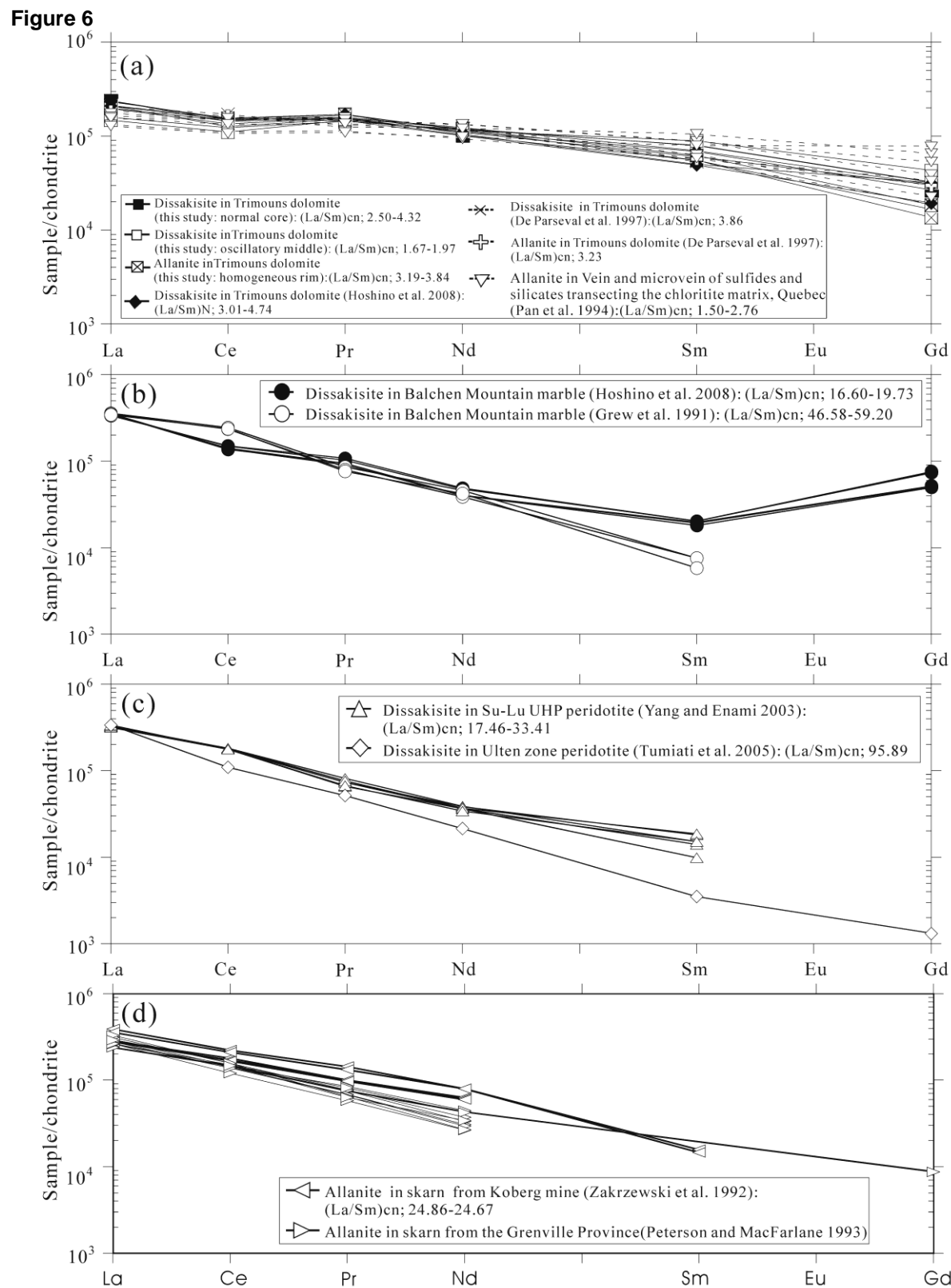


Fig. 6 Plots of chondrite-normalized REE concentrations (as determined by electron-microprobe analysis) as a function of REE: (a) dissakisite and allanite in dolomite from Trimous (De Parseval et al. 1997; Hoshino et al. 2008; this study) and both vein and microvein of sulfides and silicates transecting the chloritite matrix, Mattagami Lake mine (Pan et al. 1994), (b) dissakisite in marble from Balchen Mountain (Grew et al. 1991; Hoshino et al. 2008), (c) dissakisites in peridotite from Su-Lu UHP metamorphic terrane (Yang and Enami 2003) and Ulten zone (Tumiati et al. 2005), and (d) allanites in both skarn from Koberg mine (Zakrzewski et al. 1992) and calcite vein from the Grenville Province (Peterson and MacFarlane 1993; Sm: below detection limit). Chondrite concentrations are taken from McDonough and Sun (1995).